Silicon (2024) 16:3217–3231
https://doi.org/10.1007/s12633-024-02916-x

RESEARCH

Optimization and Kinetic Analysis of Direct Alkali Leaching of Silica from Vanadium-Bearing Shale Leaching Residue

Xuanxiong Kang[1] · Guohua Ye[1] · Siqin Zhu[1] · Yiyang Rong[1] · Changxu Song[1] · Xinyue Xiang[1] · Yun Zhang[1]

Received: 17 November 2023 / Accepted: 13 February 2024 / Published online: 22 February 2024

Abstract
The Response Surface Methodology was employed to optimize the leaching parameters for SiO_2 during NaOH alkaline leaching from vanadium acid leaching residues. The kinetic aspect of the process was also investigated. The results illustrate that each factor positively influences the SiO_2 leaching rate, with the significance of these factors ranking as follows: leaching temperature > alkali residue mass ratio > leaching duration. Under these optimal circumstances, the SiO_2 leaching rate can attain a value as high as 95.55%. A kinetic examination of the alkaline leaching process implies that the reaction process is predominantly governed by internal diffusion. The apparent activation energy of the reaction is 11.92 kJ·mol^{-1}. The kinetic equation is: $1 + 2(1 - x) - 3(1 - x)^{\frac{2}{3}} = 10.82\exp(-\frac{1192}{RT})t$, and the reaction order of NaOH is 0.7284.

Keywords Vanadium-bearing shale · Alkaline leaching · Silica · Response surface methodology · Leaching kinetics

1 Introduction

Vanadium is an important metal with widespread applications in various sectors of the national economy [1–3]. China holds the leading position in both vanadium production and consumption globally. Notably, vanadium-bearing shale accounts for 87% of China's vanadium reserves, surpassing the combined reserves of other countries worldwide [4]. Consequently, the development and utilization of vanadium-bearing shale resources hold significant importance for China's vanadium industry. Currently, acid leaching represents the predominant method employed for extracting vanadium from vanadium-bearing shale resources. However, due to the generally low vanadium content in the shale (typically ranging from 0.1% to 2.0%), the acid leaching process inevitably generates a substantial quantity of acid leaching slag, hereinafter referred to as acid leaching slag [5, 6]. If large amounts of acid leaching residue are completely stored and landfilled, it not only occupies substantial land area but also poses potential threats to soil and water resources, thereby impacting the industrial development of vanadium extraction from vanadium-bearing shale. Given these circumstances, the current research hotspot revolves around exploiting the key physical and chemical properties of acid leaching residue to achieve reduction and resource utilization, thereby promoting efficient and sustainable development within the vanadium extraction industry.

Currently, the treatment of acid leaching residue is primarily focused on the production of building materials such as ceramsite and geopolymer [7, 8]. However, the low reactivity of acid leaching residue often requires high-temperature roasting for activation or the addition of significant amounts of non-renewable clay as additives when used in building material preparation. This process is associated with challenges including a relatively lengthy duration, high production costs, and relatively low added value of the resulting products. Acid leaching residue typically contains a SiO_2 content of over 80%, making it an ideal silicon source for silicon-based materials. The main research direction for the value-added utilization of silicon-containing solid waste involves leaching silica from high-silicon solid waste to produce silica, silica aerogel, ordered mesoporous silica, zeolite, sodium metasilicate, and other silicates and compounds [9]. In order to utilize low-grade high-sulfur bauxite, Wu et al. [10] first employed suspension calcination for desulfurization and subsequently conducted NaOH alkali leaching desilication tests on the calcined bauxite under atmospheric pressure. Optimal conditions allowed for the removal of 44.9%

✉ Guohua Ye
ghye581@kust.edu.cn

[1] Faculty of Land Resource Engineering, Kunming University of Science and Technology, Kunming 650093, the People's Republic of China

of silicon. Mu et al. [11] investigated the high-concentration alkali leaching process for silicon extraction from laterite nickel ore, achieving an extraction rate of 89.89% under optimal conditions. Wang et al. [12] focused on the kinetics of alkali-soluble SiO_2 using slag as a raw material after extracting Al_2O_3 from fly ash. Under optimal conditions, the leaching rate of SiO_2 reached 95.66%. The overall leaching process follows the shrinking core model and is controlled by internal diffusion through the solid product layer. Hence, investigating the alkali dissolution and desilication process of acid leaching residue from shale vanadium extraction can address issues such as low effective utilization rate, land occupation, and soil contamination. This research can enhance the comprehensive utilization value of acid leaching residue and yield substantial economic benefits. However, there is currently limited research on the alkali dissolution process and kinetic mechanism of acid leaching residue from shale vanadium extraction, underscoring the need for in-depth exploration.

This study utilizes acid leaching residue as the primary material and applies NaOH alkaline leaching treatment to extract SiO_2 from it. The study investigates the effects of the mass ratio of NaOH to acid leaching residue, leaching temperature, leaching time, and liquid–solid ratio on the leaching rate of SiO_2 in the residue. The optimization of SiO_2 leaching rate parameters was carried out utilizing the response surface methodology. Moreover, the release kinetics of SiO_2 in acid leaching residues during NaOH alkali dissolution were thoroughly examined. The aim of this investigation was to offer a robust theoretical foundation for the multifaceted development and utilization of acid leaching residue in the process of shale vanadium extraction.

2 Materials and Methods

2.1 Material Characterization

The acid-leaching residue was obtained from Shangluo, Shaanxi, China Province, and was derived from the sulfuric acid leaching of vanadium shale ore crushed to a -4 mm particle size. The resulting residue exhibited a granular, black coloration. The residue has a granular shape and appears gray-black in color. Prior to the extraction process, tthe acid leaching residue and water were subjected to two wash cycles using a specific ratio, with the objective of achieving a near-neutral pH for the acid leaching residue. Following this, the material underwent ball milling treatment until it reached a particle size of -74 μm. Subsequently, it was mixed for SiO_2 extraction through alkali leaching. Table 1 provides the results of the main chemical multi-element analysis, while Figs. 1 and 2 depict the X-ray diffraction (XRD) and scanning electron microscopy (SEM) images, respectively.

Table 1 reveals that the primary chemical component present in the acid leaching residue from shale vanadium extraction is SiO_2, accounting for 86.88% of the composition. Additionally, it contains a certain amount of Al_2O_3, comprising 2.49% of the residue. Other components, such as CaO, MgO, and K_2O are also present. Based on the chemical composition, it is evident that the acid leaching residue is rich in SiO_2, making it a valuable raw material for silicon extraction and classifying it as a typical high-silicon industrial solid waste. The dominant mineral phase observed in Fig. 1 is quartz, characterized by numerous diffraction peaks with narrow, symmetrical shapes and strong intensity, indicating a high degree of crystallinity in the silica. Combining the chemical composition analysis, it can be inferred that the silicon component in the vanadium tailings predominantly exists in the form of quartz minerals, while the aluminum component primarily exists as albite minerals. From the analysis of Fig. 2a, it is evident that the layer or frame structure of feldspar aluminosilicate minerals aligns with the XRD results for feldspar. Typically, feldspar particles exhibit irregular granular characteristics, and in the tailings, they are distributed along the

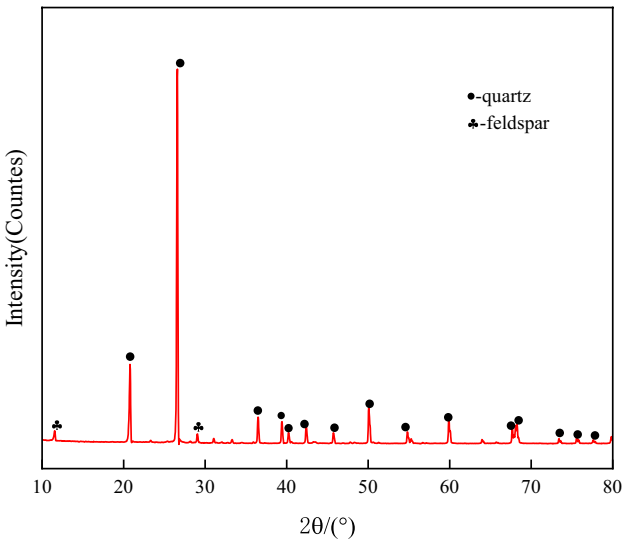

Fig. 1 XRD analysis spectrum of vanadium tailings

Table 1 Main chemical components of acid leaching residue of shale vanadium extraction%

Chemical components	SiO_2	Al_2O_3	CaO	Fe	MgO	K_2O	V_2O_5	S	P_2O_5
Content/%	86.88	2.49	1.28	0.78	0.41	0.39	0.06	1.17	0.06

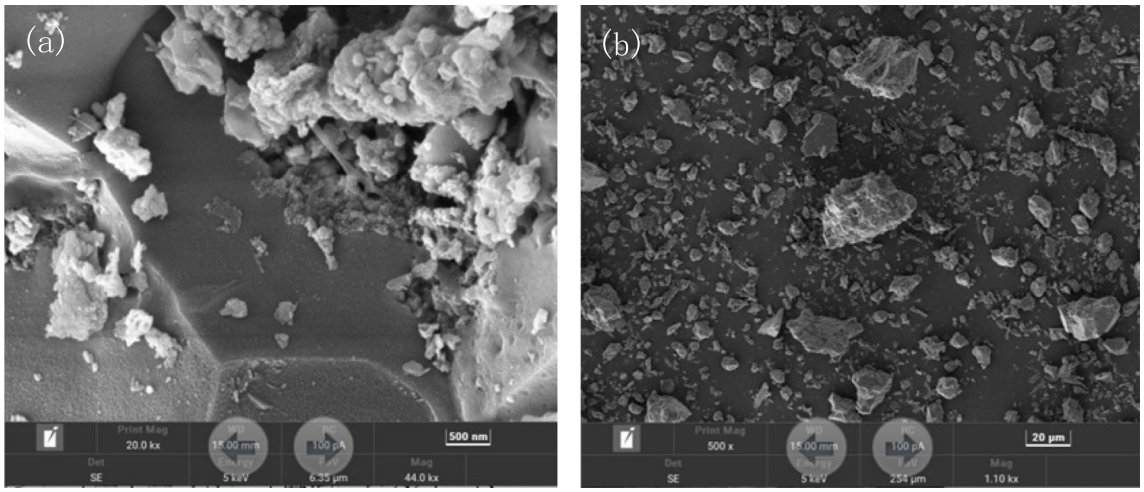

Fig. 2 SEM of acid leaching residue of shale vanadium extraction

edges of quartz particles, embedded or enveloped within quartz crystals, and arranged in a stacked manner. Furthermore, as depicted in the SEM images in Fig. 2b the acid-leaching residue consists of irregular blocky or flake particles with rough surfaces and varying sizes. Combined with the chemical composition analysis and XRD diagram, it is evident that most of the silicon in the acid leaching residue exists in the form of quartz (SiO_2), characterized by high crystallinity. The particle surfaces also feature some pores, which facilitate effective leaching when subjected to NaOH treatment.

2.2 Methods

2.2.1 Leaching Tests

A specific quantity of acid leaching residue was introduced into the reaction vessel, followed by the addition of NaOH in a predetermined ratio. The reaction vessel was sealed and placed inside a heating sleeve. The control system was utilized to set the reaction temperature and duration. Once the reaction was completed, the hot filtrate was filtered, and the SiO_2 content in the filtrate was determined using silicon molybdenum blue spectrophotometry. Subsequently, the leaching rate x was calculated using the following method:

$$x = \frac{c \times V}{w \times m} \times 100\% \quad (1)$$

where x denotes the leaching rate of SiO_2, c denotes the concentration of SiO_2 in the filtrate(g/L), V represents the volume of the filtrate (L), m represents the mass of the acid leaching residue (g), and w represents the grade of SiO_2 in the acid leaching residue (%).

2.2.2 Experimental Design and Statistical Analysis

In accordance with the procedure outlined in Section 2.2.1, the impact of the alkali slag mass ratio, leaching temperature, leaching time, and liquid–solid ratio on the leaching rate of SiO_2 was investigated using a single-factor approach. Subsequently, the response surface methodology was employed to optimize the process. The response surface methodology is a mathematical and statistical optimization technique that utilizes regression analysis to establish the relationship between factors and response variables in multifactor experiments. It facilitates the evaluation of influential factors and their interactions, enabling the determination of optimal factor levels to achieve the optimal response value [13, 14]. Given the complex nature of the SiO_2 extraction process from acid leaching residue through alkali leaching, the response surface method provides a rapid and accurate means to identify the optimal reaction conditions.

For the experimental analysis, Design-Expert 13 software was utilized. Based on the results of the single-factor tests, the alkali slag mass ratio, leaching temperature (K), and leaching time (min) were identified as significant factors affecting the leaching rate of SiO_2 and denoted as A, B, and C, respectively. The leaching rate of SiO_2 was selected as the evaluation criterion. The experimental factor levels and their corresponding codes are presented in Table 2.

2.2.3 Kinetic Analysis of Silica Leaching

Leaching kinetics analysis plays a vital role in determining the extent of leaching reactions, assessing the impact of factors such as temperature and alkali slag ratio on the

Table 2 Different factor values and horizontal coding of response surface design

Factors	Notation	Range of level		
		-1	0	1
Alkali residue mass ratio	A	1	1.25	1.5
Leaching temperature/K	B	453.15	473.15	493.15
Leaching time/min	C	60	90	120

reaction rate, and identifying the rate-controlling step [15]. The leaching process of the acid leaching residue sample represents a typical non-catalytic heterogeneous solid–liquid reaction. Initially, the reaction initiates at the surface of the solid material and gradually progresses toward the interior. A distinct interface is observed between the raw material and the product. As the reaction proceeds over time, the solid reactant diminishes in size until it eventually disappears. Hence, the unreacted core reduction model is employed [16]. The rate-controlling steps within the unreacted core reduction model encompass chemical reaction control, internal diffusion control, and mixed control, as depicted in Eqs. (2-4) [17]. By fitting the experimental data, it becomes possible to determine the rate-controlling steps of the leaching reaction.

$$1-(1-x)^{1/3=}k1t(controlled\ by\ chemical\ reaction) \tag{2}$$

$$1-2(1-x)-3(1-x)^{2/3=}k2t(pore\ diffusion\ control) \tag{3}$$

$$(1-x)^{-1/3}-1+1/3ln(1-x)=k_3t(hybrid\ control) \tag{4}$$

where x-vanadium leaching rate; t-leaching time; k_n ($n=1,2,3$) -leaching rate constants.

The apparent activation energy of the leaching reaction provides valuable insights into the impact of temperature variations on the leaching rate, serving as a critical criterion for determining the rate-controlling steps. By employing the Arrhenius formula (5), we can derive Eq. (6) to elucidate this relationship.

$$k=B\exp(-\frac{E_a}{RT}) \tag{5}$$

$$lnk=-\frac{E_a}{RT}+lnB \tag{6}$$

Where B is the frequency factor; E_a is the apparent activation energy of the reaction, kJ·mol^{-1}; R is the gas constant, 8.314 kJ·mol^{-1}; T is the thermodynamic temperature, K.

3 Results and Discussion

3.1 Single Factor Leaching Tests

To optimize the alkali leaching conditions for SiO_2, a specific acid leaching residue was chosen for a single-factor experiment. The study investigated the impacts of the alkali slag mass ratio, leaching temperature, leaching time, and liquid–solid ratio on the leaching rate of SiO_2. The results are presented in Fig. 3. The primary reaction of the acid leaching residue in the NaOH solution is illustrated by Eq. 7.

$$SiO_2+NaOH\rightarrow Na_2SiO_3+H_2O \tag{7}$$

In Fig. 3(a), it is evident that the leaching rate of silica rises as the alkali slag mass ratio increases. The highest leaching rate of silica is achieved when the mass ratio of alkali slag reaches 1.25:1. This phenomenon arises from the augmentation of alkali concentration within a defined range, which in turn elevates the OH- concentration. Consequently, it expedites the rupture of Si–O chemical bonds in the acid leaching residue and markedly amplifies the dissolution of SiO_2 [18, 19]. Beyond this ratio, further increases in the mass ratio of alkali slag do not significantly enhance the leaching rate of silica. This behavior can be attributed to the improved contact between hydroxide ions in the solution and the surface of acid leaching residue particles at higher sodium hydroxide concentrations, leading to a more efficient reaction. However, once the maximum contact is achieved, the leaching rate of silica no longer increases with higher sodium hydroxide concentrations [20]. From an economic standpoint, the optimal alkali-slag ratio for leaching silica from acid leaching residue is determined to be 1.25:1.

Figure 3(b) indicates that the leaching rate of SiO_2 exhibits a significant increase within the temperature range of 413.15 to 473.15 K. This trend indicates that higher temperatures facilitate enhanced diffusion and reaction rates between mineral particles and the leaching agent, thereby improving the leaching effectiveness. The leaching rate reaches its peak when the temperature reaches 473.15 K. Research indicates that in a solid–liquid reaction system, an increase in temperature enhances the thermal motion of molecules, and also promotes the transition of non-activated molecules into activated molecules, leading to more molecules participating in the reaction and accelerating the reaction rate. As a result, the leaching temperature increases, and the leaching rate of silicon dioxide in the acid leaching residue is increased [21]. However, excessively high leaching temperatures may also inhibit the leaching of silicon dioxide in the acid leaching residue.This may be attributed to the formation of larger aggregates formed by fused sodium silicate clusters at

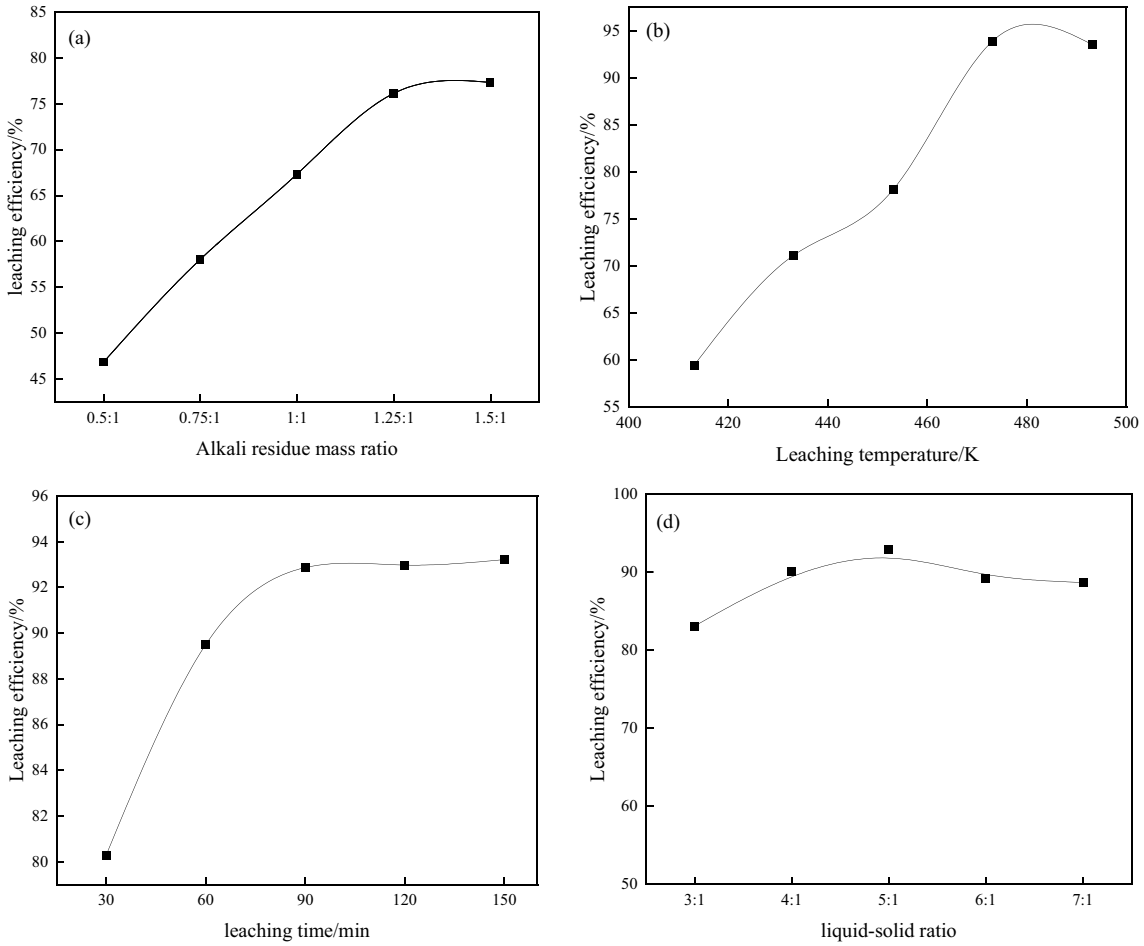

Fig. 3 **a** Influence of alkali-slag mass ratio on SiO_2 leaching rate (conditions: liquid–solid ratio 5:1, alkali leaching temperature 453.15 K, leaching time 90 min, stirring speed 500 rpm). **b** Impact of leaching temperature on silica leaching efficiency (conditions: alkali residue ratio 1.25:1, liquid–solid ratio 5:1, leaching time 90 min, stirring speed 500 rpm). **c** Effect of leaching time on silica leaching efficiency (conditions: alkali residue ratio 1.25:1, liquid–solid ratio 5:1, leaching temperature 473.15 K, stirring speed 500 rpm). **d** Influence of liquid–solid ratio on silica leaching efficiency (conditions: alkali residue ratio 1.25:1, leaching temperature 473.15 K, leaching time 90 min, stirring speed 500 rpm)

excessively high temperatures, which coat the surface of unreacted acid leaching residue and hinder the reaction. Consequently, the appropriate leaching temperature is determined to be 473.15 K.

Regarding Fig. 3(c), the leaching rate of silica increases with prolonged leaching time until reaching 90 min. Longer leaching times enhance the probability of collision between hydroxide ions and quartz particles, leading to higher leaching rates [22]. However, after 90 min, the leaching rate of silica tends to reach a plateau. This is indicative of the reaction reaching an equilibrium state under these conditions, making further enhancement difficult. Therefore, from a process perspective, the optimal leaching time for acid leaching residue is determined to be 90 min.

As observed in Fig. 3(d), the leaching rate of silica initially increases and then decreases with an increase in the liquid–solid ratio. This behavior can be attributed to the following factors. When the liquid–solid ratio is low, the slurry viscosity becomes high, impeding sufficient contact between SiO_2 in the acid leaching residue and OH^- in the solution. Consequently, increasing the liquid–solid ratio to a certain extent enhances the fluidity of the slurry, promoting more thorough contact between SiO_2 and OH^- [23, 24]. However, when the liquid–solid ratio continues to rise, the concentration of OH^- in the solution decreases, leading to a reduced collision frequency between OH^- and SiO_2 in the reactor. This decrease in collision frequency adversely affects the leaching of silica, resulting in a decline in the leaching rate. Therefore, a liquid–solid ratio of 5:1 is chosen as the optimal condition.

3.2 Modeling and Statistical Analysis

3.2.1 Response Surface Design and Results

Building upon the single-factor experiment, the present study focuses on three key factors that influence the leaching rate of SiO_2: alkali residue mass ratio, leaching temperature, and leaching time. To systematically explore the effects of these factors, the Box-Behnken optimization method was employed to design an experimental plan consisting of three factors and three levels. A total of 17 experimental points were conducted [25]. The outcomes of these experiments are presented in Table 3.

Table 3 Box-Behnken experimental design matrix and results

Run	A	B	C	SiO_2/%
1	1	453.15	90	73.21
2	1.5	453.15	90	77.98
3	1	493.15	90	85.32
4	1.5	493.15	90	92.98
5	1	473.15	60	80.92
6	1.5	473.15	60	90.41
7	1	473.15	120	86.81
8	1.5	473.15	120	93.91
9	1.25	453.15	60	70.87
10	1.25	493.15	60	85.2
11	1.25	453.15	120	79.2
12	1.25	493.15	120	92.81
13	1.25	473.15	90	92.91
14	1.25	473.15	90	93.30
15	1.25	473.15	90	93.90
16	1.25	473.15	90	92.98
17	1.25	473.15	90	92.10

3.2.2 Establishment of Regression Model and Significance Analysis

By employing Design-Expert 13 software, the data from Table 3 were subjected to multiple regression analysis to establish a quadratic polynomial regression equation. This equation relates the SiO_2 leaching rate to the mass ratio of alkali slag, leaching temperature, and leaching time. The resulting equation is as follows:

$$Y = 93.04 + 3.63A + 6.88B + 3.17C + 0.7225AB - 0.5975AC - 0.1800BC - 2.34A^{2-}8.33B^{2-}2.69C^2 \quad (8)$$

Table 4 presents the results of the significance test and variance analysis conducted for the model.

Table 4 reveals several key findings. Firstly, the F-value of the model is 78.26, indicating its significance. Additionally, the p-value for lack of fit is 0.0592, which is greater than the significance level of 0.05, suggesting that the lack of fit is not significant. The determination coefficient, R^2, is calculated to be 0.9902, indicating a strong agreement between the predicted and observed values for silica leaching rate. Moreover, the adjusted determination coefficient, R^2_{Adj}, is 0.9775, indicating that the model can explain approximately 97.75% of the variance in the silica leaching rate. The model demonstrates a high level of accuracy and a small error. Both the coefficient of variation (CV) and the signal-to-noise ratio serve as measures of the model's accuracy. A lower coefficient of variation and a higher

Table 4 Variance analysis of regression equation

Source	Sum of Squares	df	Mean Square	F-value	*p*-value	
Model	938.14	9	104.24	78.26	< 0.0001	significant
A-Alkali residue mass ratio	105.27	1	105.27	79.04	< 0.0001	
B-Leaching temperature	378.81	1	378.81	284.41	< 0.0001	
C-Leaching time	80.20	1	80.20	60.21	0.0001	
AB	2.09	1	2.09	1.57	0.2508	
AC	1.43	1	1.43	1.07	0.3349	
BC	0.1296	1	0.1296	0.0973	0.7642	
A^2	22.99	1	22.99	17.26	0.0043	
B^2	292.09	1	292.09	219.30	< 0.0001	
C^2	30.45	1	30.45	22.86	0.0020	
Residual	9.32	7	1.33			
Lack of Fit	7.61	3	2.54	5.93	0.0592	not significant
Pure Error	1.71	4	0.4278			
Cor Total	947.46	16				

R^2:0.9902, R^2_{Adj}:0.9775, CV:1.33, Adeq Precision:25.3250

signal-to-noise ratio indicate greater experimental accuracy. In this case, the coefficient of variation is 1.33%, and the signal-to-noise ratio is 25.325, affirming the high accuracy of the quadratic model [26]. Therefore, this model can effectively analyze and predict the process of silica separation from acid leaching tailings in shale vanadium extraction.

3.2.3 Response Surface Analysis and Optimization

The response surface plot serves as a valuable tool for analyzing the impact and interaction of different factors, aiding in the determination of optimal process conditions. By considering the influence of various factors and their interactions on the leaching efficiency of SiO_2, response surface, and contour maps were generated. These graphical representations are presented in Fig. 4.

The shape of the response surface and contour plots provides insights into the influence of experimental factors and the significance of their interactions. Steeper surfaces indicate more significant factor influences, while flatter surfaces suggest less pronounced effects. Additionally, the contour shape and surface curvature can be utilized to determine the significance of factor interactions. Elliptical contours and larger surface curvatures indicate more pronounced factor interactions, whereas circular contours and smaller curvatures suggest less significant interactions [27]. Analyzing Fig. 4(a) and (b), it is observed that within a certain range, the leaching rate of SiO_2 increases with an increase in the alkali slag mass ratio and leaching temperature. Notably, the effect of leaching temperature is more prominent than that of the alkali slag mass ratio. As the leaching temperature or alkali slag mass ratio continues to increase, the impact on the leaching rate of SiO_2 diminishes, indicating the presence of an optimal region for the alkali slag mass ratio and leaching temperature that maximizes the synergistic leaching effect. The contour plots and surface curvatures demonstrate that the interaction between the alkali slag mass ratio and leaching time is not significant. Similar conclusions can be drawn from Fig. 4(c)-(f), aligning with the observations in Fig. 4(a) and (b). The leaching rate of SiO_2 increases with an increase in the alkali slag mass ratio and decreases when it exceeds a certain range. This suggests the existence of an optimal parameter combination within the experimental design range that maximizes the leaching rate of SiO_2. Based on the shape of the surface and contour plots, it is evident that the interaction between the alkali slag mass ratio and leaching temperature, as well as between the alkali slag mass ratio and leaching time, is not significant.

In summary, in conjunction with the results of variance analysis, it is evident that all variables exert a significant influence on the leaching rate of vanadium, while the interactions between variables are not significant. The order of the influence of the three preparation factors on the leaching efficiency of silica is as follows: leaching temperature (B) > alkali slag ratio (A) > leaching time (C).

3.2.4 Determination of Process Conditions

Based on the above model, the leaching conditions for extracting silica from acid leaching residue were optimized by Design-Expert13 software and over 100 solutions were suggested. Taking into account various factors, including energy consumption, NaOH dosage, and silica leaching rate, the outcomes of selecting the most favorable conditions are depicted in Fig. 5.

Considering the equipment limitations, the optimal conditions were adjusted accordingly. The adjusted conditions for extracting SiO_2 from vanadium tailings were as follows: a leaching temperature of 480.13 K, a reaction time of 96 min, an alkali residue mass ratio of 1.34, a liquid–solid ratio of 5:1, and a rotation speed of 500 rpm. Under these conditions, the achieved leaching rate was 95.55%. The actual results align closely with the predicted outcomes, indicating the reasonableness and feasibility of optimizing the process conditions for SiO_2 extraction from vanadium tailings using response surface methodology. Additionally, under these leaching conditions, the release of acid leaching residue can be diminished by 89.7%. This process not only enables the conversion of silica into an alkali-soluble form, thereby increasing its value, but also significantly mitigates the discharge of acid leaching residue, addressing various issues stemming from inadequate tailings pond and tailings storage.

3.3 Microstructure Evolution of Leaching Residue

By employing a leaching temperature of 480.13 K, a reaction time of 96 min, an alkali residue mass ratio of 1.34, a liquid–solid ratio of 5:1, and a rotation speed of 500 rpm, the optimal alkali leaching process was achieved, resulting in the formation of high-quality silicon residue and leaching silicon solution. The obtained leaching residues were characterized using XRD, SEM and chemical multi-element analysis techniques, while the elements present in the alkali leaching solution were analyzed using ICP. The obtained results are presented in Fig. 9, Fig. 10, Tables 5 and 6, respectively.

Figure 6 reveals notable differences between the XRD spectra before and after leaching. The appearance of new diffraction peaks and the weakening or disappearance of main mineral peaks are observed. Following NaOH alkali

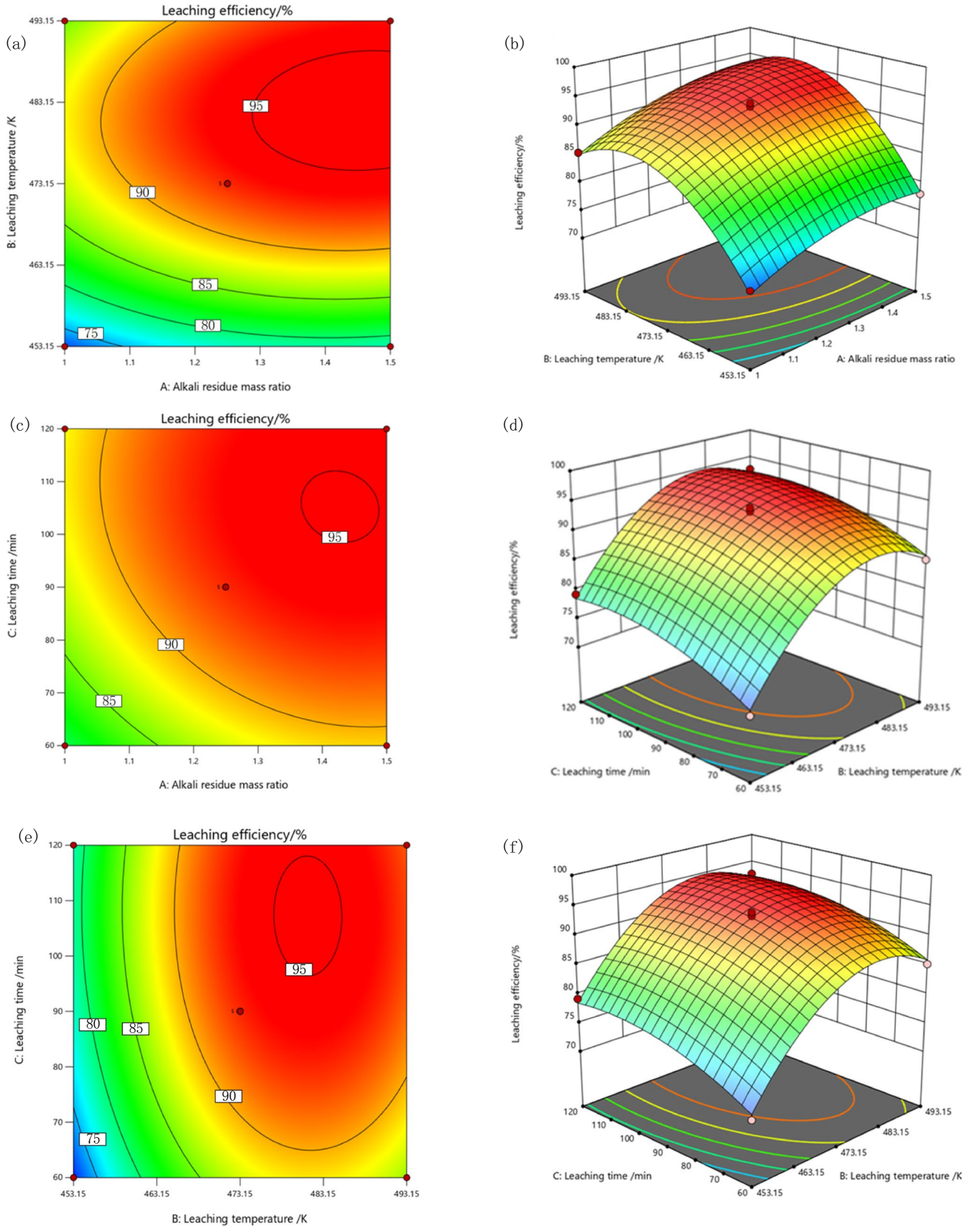

Fig. 4 Title Response surface and contour plots for silica leaching efficiency: **a** A – B contour plot; **b** A – B response surface; **c** A – C contour plot; **d** A – C response surface; **e** B – C contour plot; **f** B – C response surface

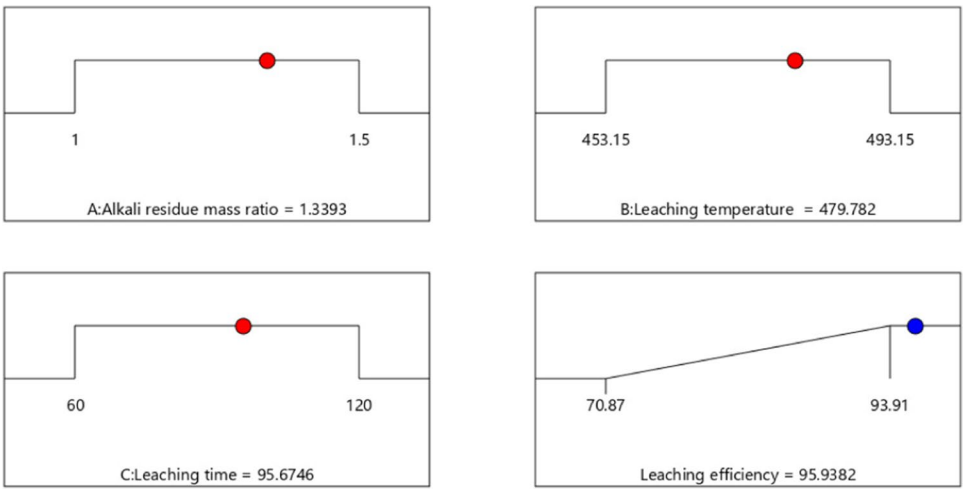

Fig. 5 Model optimal process

Table 5 The main chemical components in alkaline leaching residue%

Chemical components	SiO_2	Al_2O_3	CaO	Fe	MgO	V_2O_5	S
Content/%	37.51	5.64	18.92	12.02	6.86	0.23	12.56

Table 6 The main elements in alkali leaching solution%

Chemical element	Si	Na	Al	Fe	P
Content/g·L^{-1}	46.43	100.74	0.12	0.02	0.01

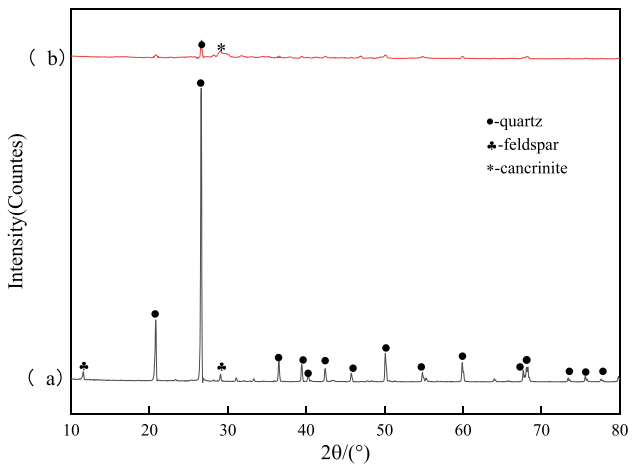

Fig. 6 XRD patterns of samples before and after leaching (**a**) residue and (**b**) solid phase after alkali leaching

leaching, a low-intensity diffraction peak of nepheline emerges, while the diffraction peaks of quartz and feldspar experience a significant decrease or complete disappearance. This indicates the relatively complete reaction between silicon dioxide and sodium hydroxide in the acid leaching residue, with only a small residue of silicon dioxide and a limited amount of silicon converting into nepheline. These findings align with the previously observed high leaching rate of silica, confirming that nearly all of the silicon in the tailings enters the solution. The SEM analysis in Fig. 7 demonstrates the absence of visible quartz and feldspar. A comparison with the SEM image in Fig. 2 clearly reveals extensive particle breakage in the acid-leaching slag, increased porosity in the alkaline leaching slag, and significant damage to the mineral structure. This further validates the substantial dissolution of SiO_2 in minerals in the NaOH solution. Table 5 illustrates that the proportion of SiO_2 components in the residue after alkaline leaching of silicon from the acid leaching residue is 37.51%, while the proportions of Al_2O_3, CaO, and Fe are 5.64%, 18.92%, and 12.02%, respectively. The mass of the alkaline leaching residue after combined alkaline leaching accounts for only 10.3% of the mass of the acid leaching residue, indicating nearly complete leaching of silica from the acid leaching residue. However, only a small fraction of Al_2O_3 is leached into the solution, with minimal impact on the subsequent preparation of silicon-based products, while CaO and Fe are almost not leached. Analysis of Table 5 reveals that the alkaline leaching solution predominantly comprises significant quantities of Si and Na elements, while the presence of other metal elements is negligible, aligning with the observations made through XRD, SEM, and chemical multi-element analysis of the alkaline leaching residue.

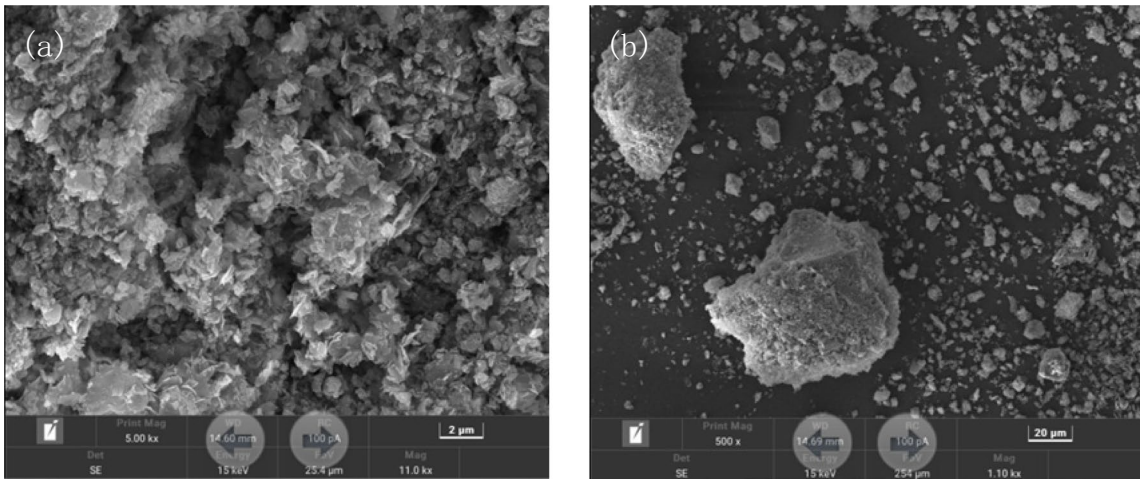

Fig. 7 SEM image of acid leaching residue alkali leaching silicon tailings

3.4 Leaching Kinetics of Silica

3.4.1 Silica Leaching Control Steps

To determine the control steps of the leaching process, further investigations were conducted to assess the impact of different temperatures on the leaching efficiency under optimal conditions. The effects of temperatures ranging from 443.15 K to 473.15 K on leaching efficiency were studied. Figure 8 illustrates the relationship between silica leaching efficiency (x) and time (t) at various temperatures.

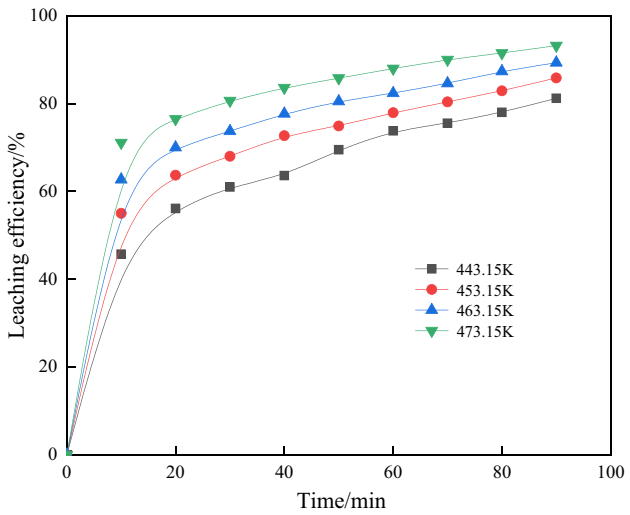

Fig. 8 Relationship between time and leaching efficiency at different temperatures

Figure 8 demonstrates the impact of temperature on the extraction of silicon dioxide through alkali leaching of acid leaching residue. Lower temperatures result in noticeably lower leaching efficiency, while increasing the leaching temperature enhances the leaching efficiency of silicon dioxide to a certain extent. This observation aligns with the findings of previous experiments, highlighting the substantial influence of temperature on silicon dioxide leaching efficiency. To determine the rate control step of the leaching process, the data from Fig. 8 were utilized in the kinetic equations for chemical reaction control, mixing control, and diffusion control. By analyzing the linear relationship between the plotted lines and time (t), the rate control step of the reaction was identified. The results are presented in Fig. 9 and Table 7.

The correlation coefficient (R^2) obtained from fitting the data aligns closely with 1, indicating a stronger linearity and a better fit to the actual leaching kinetics of the control process. Combining the findings from Fig. 9 and Table 6, it is evident that within the temperature range of 443.15 K to 473.15 K, there is a stronger linear correlation between $1+2(1\text{-}x)\text{-}3(1\text{-}x)^{2/3}$ and time (t). This suggests that the control step for extracting silica from acid leaching residue belongs to diffusion control [28]. To determine the apparent activation energy, the relationship between ln(k) and 1/T was plotted using the Arrhenius formula. The fitted result is presented in Fig. 10 (the equation shown in the figure represents the fitted straight line, with y representing the ordinate in each figure and x representing the abscissa).

From Fig. 10, it is evident that there is a strong linear relationship between ln(k) and 1/T. By using the fitted linear

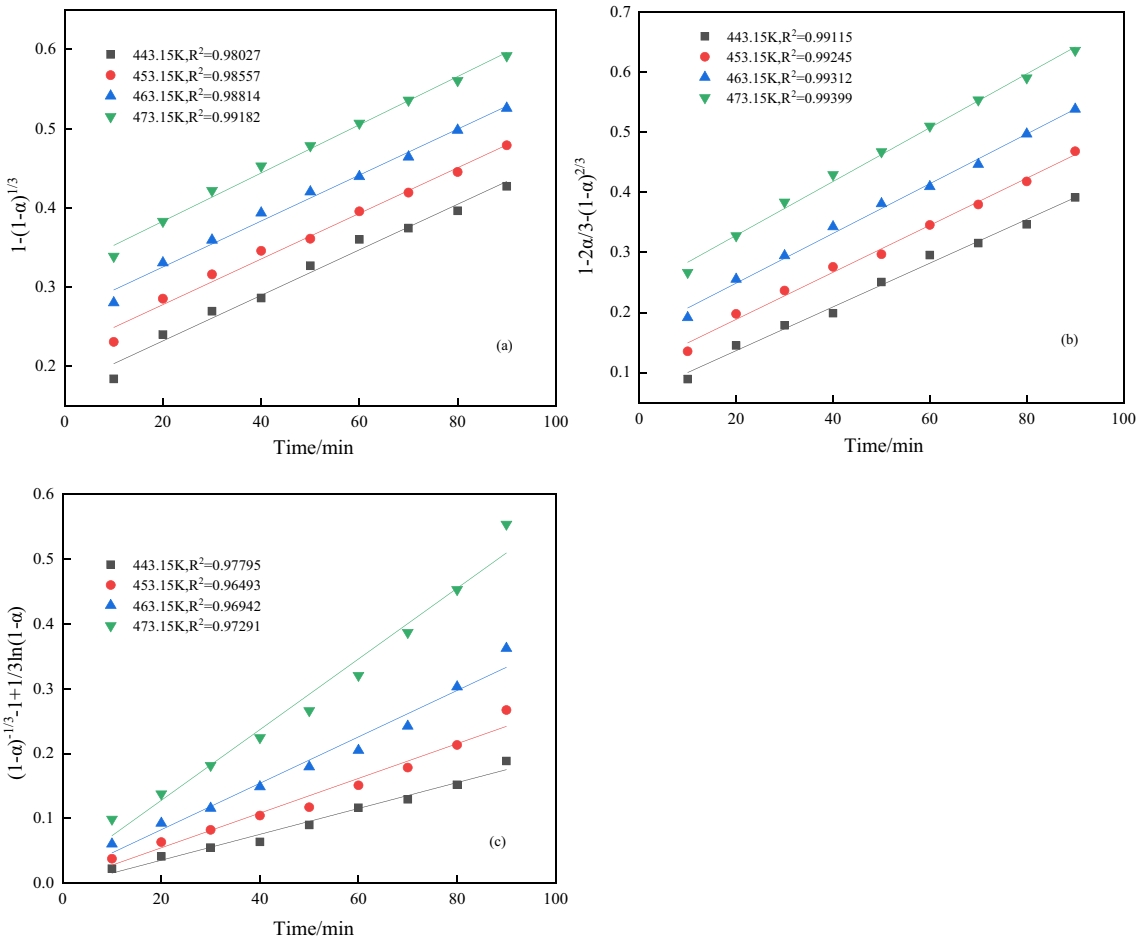

Fig. 9 **a** The relationship between $1\text{-}(1\text{-}x)^{1/3}$ and time at different temperatures. **b** The relationship between $1+2(1\text{-}x)\text{-}3(1\text{-}x)^{2/3}$ and time at different temperatures. **c** The relationship between $(1\text{-}x)^{-1/3}\text{–}1+1/3\ \ln(1\text{-}x)$ and time at different temperatures

Table 7 Apparent rate constants and correlation coefficients at different temperatures

Temperature/K	$1\text{-}(1\text{-}x)^{1/3}$		$1+2(1\text{-}x)\text{-}3(1\text{-}x)^{2/3}$		$(1\text{-}x)^{-1/3}+1/3\ \ln(1\text{-}x)\text{-}1$	
	$ka\bullet10^{-4}$/(min)	R^2	$k_b\bullet10^{-4}$/(min)	R^2	$k_c\bullet10^{-4}$/(min)	R^2
443.15	28.7	0.98037	36.4	0.99115	20.0	0.97795
453.15	28.5	0.98432	38.8	0.99238	26.8	0.96493
463.15	29.0	0.98814	41.4	0.99312	35.8	0.96942
473.15	30.4	0.99182	44.8	0.99399	54.6	0.97291

equation and the Arrhenius variable form, the apparent activation energy for silica extraction from acid leaching residue is calculated to be 11.92 $kJ{\cdot}mol^{-1}$. This value falls within the typical range of activation energies for diffusion control processes, which is usually between 4 and 12 $kJ{\cdot}mol^{-1}$, while the activation energy for chemical control processes is typically greater than 41.8 $kJ{\cdot}mol^{-1}$ [29–31]. The activation energy further supports the conclusion that the leaching process of SiO_2 from acid leaching residue using NaOH solution is controlled by internal diffusion within the product-free layer. Therefore, increasing the leaching temperature and liquid–solid ratio appropriately can enhance the leaching rate of silica. The frequency factor (A) is determined to be 10.82. Thus, the kinetic equation for silica extraction from acid leaching residue can be expressed as $1+2(1\text{-}x)\text{-}3(1\text{-}x)^{2/3}$.

$$1+2(1-x)-3(1-x)^{\frac{2}{3}}=10.82\ \exp(-\frac{1192}{RT})t \tag{9}$$

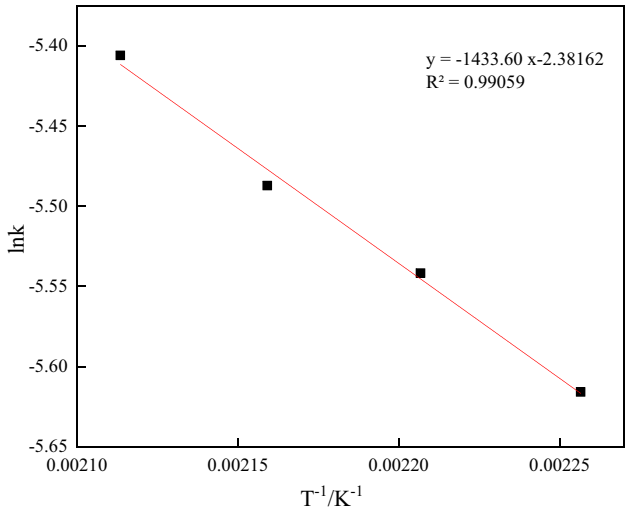

Fig. 10 Arrhenius plot of silicon extracted from acid leaching residue by alkali at 443.15–473.15 K

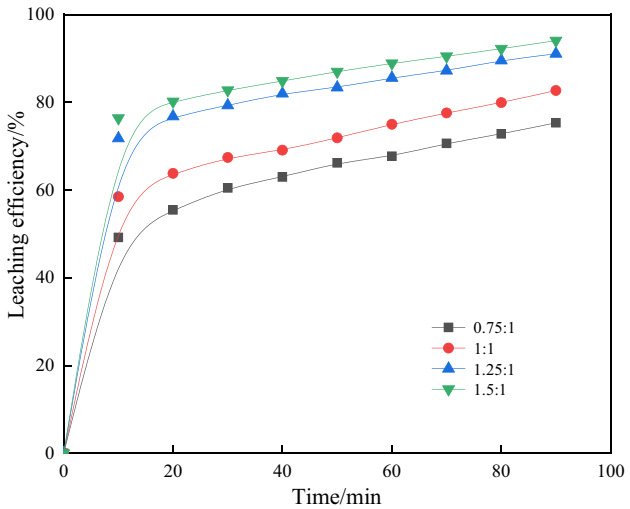

Fig. 11 The relationship between time and leaching efficiency under different mass ratios of alkali slag

3.4.2 Reaction Order of Sodium Hydroxide

The investigation was conducted to determine the reaction order of NaOH in the leaching process of acid leaching residue by examining the impact of alkali slag mass ratio on SiO_2 leaching under optimal conditions. The relationship between vanadium leaching efficiency (x) and time (t) at different temperatures is depicted in Fig. 11.

It is evident from Fig. 11 that, with the increase in the mass ratio of alkali slag, the leaching rate of silica also increases. The reaction is approximately 80% complete within the first 20 min, which aligns with the findings of previous single factor tests. To determine the reaction order of NaOH in the leaching process of acid leaching residue, the data from Fig. 11 were utilized in kinetic equations representing chemical reaction control, hybrid control, and diffusion control. The linear relationship between the leaching efficiency and time (t) was analyzed. The results are presented in Fig. 12 and Table 8.

Based on the analysis of Fig. 12 and Table 8, it is evident that the diffusion control step exhibits a higher correlation coefficient compared to other control steps, with a larger R^2 value than chemical reaction control and mixed control steps. This indicates that the leaching process of silica is primarily governed by internal diffusion across different alkali slag mass ratios. The relationship between the leaching rate (k) and alkali slag ratio (B) at various alkali slag mass ratios is represented by the linear fitting of lnk and lnB, as depicted in Fig. 13.

It can be seen in Fig. 13 that the fitted R^2 value is 0.99532, indicating a significant influence of different alkali-slag mass ratios on the apparent rate constant (k) with a non-linear relationship within a certain range. When extracting silica through alkali leaching, the apparent reaction order of sodium hydroxide is determined to be 0.7284. The coefficient of the regression value R^2 is moderate, and the liquid–solid ratio is sufficient. Thus, the reaction can be considered a pseudo-first-order reaction to a certain extent [32, 33]. Increasing the mass ratio of alkali residue appropriately enhances the dissolution of silica in acid leaching residue, thereby improving the leaching efficiency of silica. This finding aligns with the previous experimental results.

4 Conclusion

The effects of important operational parameters on alkali leaching of silicon from acid leaching residue were examined through Box-Behnken experimental optimization. The variance analysis results demonstrated that the quadratic polynomial model exhibited better fitting performance. Each factor exhibited a significant positive impact on the leaching rate of SiO_2. The alkali slag mass ratio, leaching temperature, and leaching time exerted a notable influence on the leaching rate of SiO_2, while the liquid–solid ratio had

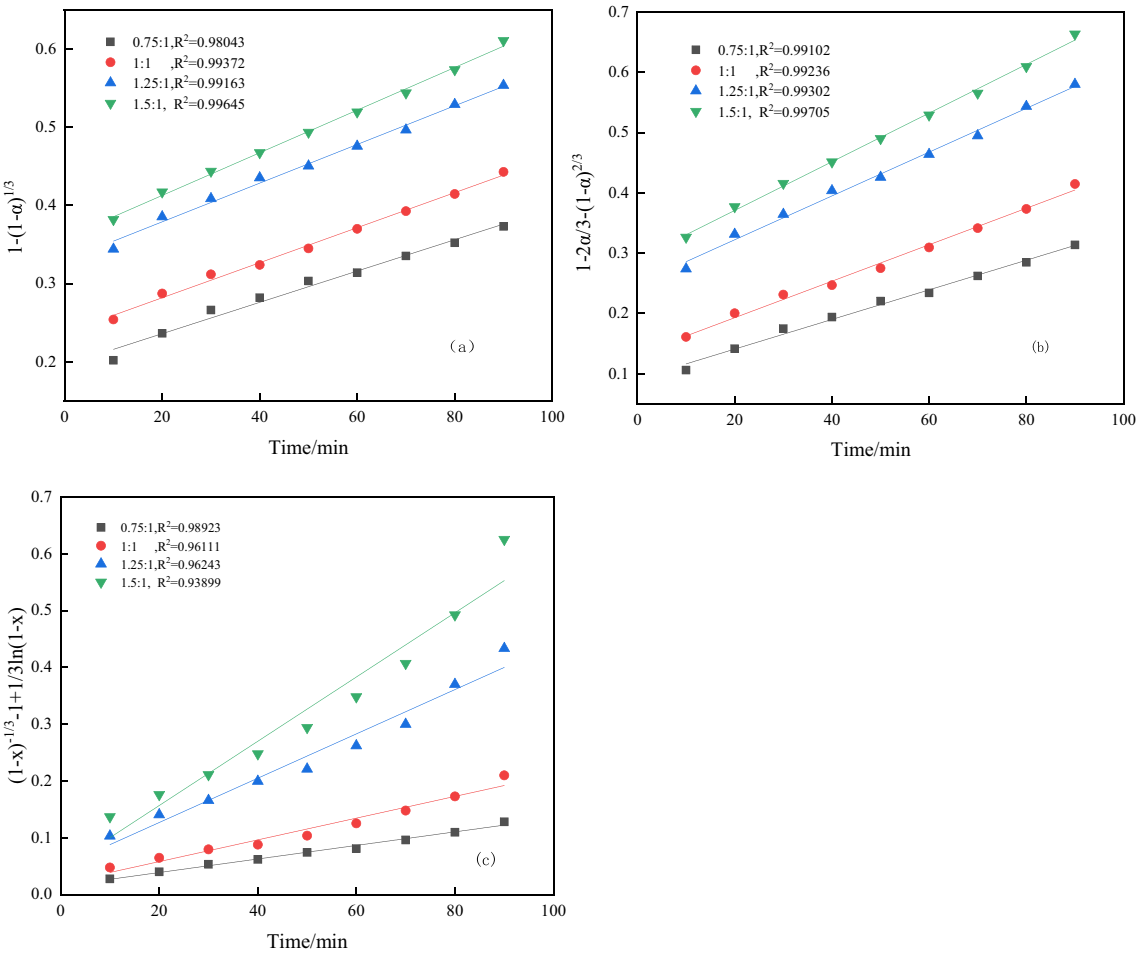

Fig. 12 **a** The relationship between $1\text{-}(1\text{-}x)^{1/3}$ and time under different alkali residue mass ratios; **b** The relationship between $1+2(1\text{-}x)\text{-}3(1\text{-}x)^{2/3}$ and time under different alkali residue mass ratios; **c** The relationship between $(1\text{-}x)^{-1/3}\text{-}1+1/3\ \ln(1\text{-}x)$ and time under different alkali residue mass ratios

Table 8 Apparent rate constants and correlation coefficients at different $NaOH/SiO_2$ mass ratios

	$1\text{-}(1\text{-}x)^{1/3}$		$1+2(1\text{-}x)\text{-}3(1\text{-}x)^{2/3}$		$(1\text{-}x)^{-1/3}+1/3\ \ln(1\text{-}x)\text{-}1$	
	$ka\bullet10^{-4}$/(min)	R^2	$k_b\bullet10^{-4}$/(min)	R^2	$k_c\bullet10^{-4}$/(min)	R^2
443.15	20.0	0.98043	24.6	0.99102	11.9	0.98923
453.15	22.4	0.99372	30.3	0.99236	19.1	0.96111
463.15	24.7	0.99163	36.4	0.99302	39.0	0.96243
473.15	27.3	0.99645	40.4	0.99705	56.6	0.93899

a minor effect. Taking into account various considerations, the optimal conditions for achieving the highest leaching efficiency of SiO_2 were determined to be a leaching temperature of 470.13 K, a reaction time of 96 min, an alkali residue mass ratio of 1.34, a liquid–solid ratio of 5:1, and a rotation speed of 500 rpm. Under these conditions, the leaching rate of SiO_2 reached 95.55%. The kinetic fitting data for the alkali dissolution reaction of acid leaching residue indicated that the alkali leaching process in this study adheres to the unreacted core reduction model, primarily controlled by external diffusion. Through kinetic model analysis, the apparent activation energy of the reaction is 11.92 kJ·mol^{-1}, and the kinetic equation can be expressed as: $1+2(1-x)-3(1-x)^{\frac{2}{3}}=10.82\exp(-\frac{1192}{RT})t$. The

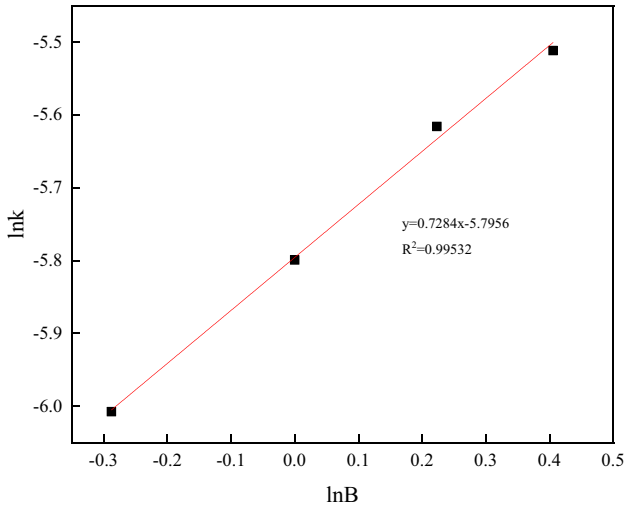

Fig. 13 Arrhenius plot of alkali leaching silicon from acid leaching residue with different alkali residue mass ratios

reaction order of NaOH is approximately 0.7284, indicating that it can be considered a pseudo-first-order reaction to a certain extent.

Acknowledgements Acknowledgements to Kunming University of Science and Technology.

Author Contributions All authors reviewed the manuscript.

Xuanxiong Kang: Conceptualization, Validation, Data curation, Formal analysis, Writing- Original draft preparation, Writing- Reviewing and Editing. Guohua Ye: Investigation, Methodology, Project administration, Resources, Supervision, Validation, Writing-review and editing. Siqin Zhu: Validation Yiyang Rong: Resources. Changxu Song: Data curation. Xinyue Xiang: Investigation. Yun Zhang: Visualization.

Funding This research was funded by National Natural Science Foundation of China (No. 51964028).

Data Availability No datasets were generated or analysed during the current study.

Declarations

Ethics Approval The research is not involving the studies on human or their data.

Consent to Participate Consent.

Consent for Publication Consent.

Competing Interests The authors declare no competing interests.

References

1. Tang Y, Ye GH, Zhang H, Kang XX, Zhu SQ, Liang XY (2022) Solvent extraction of vanadium with D2EHPA from aqueous leachate of stone coal after low-temperature sulfation roasting. Colloid surface A 650:Article 129584
2. Zhang H, Ye GH, Chen ZY, Tang Y, Tao YY, Hu YJ (2022) Complexation and activation of fluoride ion and its acceleration for dissolution of cations on the surface of vanadium-containing biotite (002). Appl Surf Sci 586:Article 152767
3. An YR, Ma BZ, Li X, Chen YQ, Wang CY, Wang BH, Gao ML, Feng GS (2023) A review on the roasting-assisted leaching and recovery of V from vanadium slag. Process Saf Environ 173:263–276
4. Kang XX, Ye GH, Zhu SQ, Liang XY, Rong YY, Song CX, Xiang XY, Zhang Y (2023) Research progress on resource utilization of vanadium-bearing shale tailings. Mod Chem Ind 04:1–8 (in Chinese with English abstract)
5. Zhang CQ, Sun CY, Li H, Yin WZ, Zhou JJ (2020) Blank roasting kinetics of illite type vanadium bearing stone coal. J Mater Res Technol 9:7363–7369
6. Zhang YM, Bao SX, Liu T, Chen TJ, Huang J (2011) The technology of extracting vanadium from stone coal in China: History, current status and future prospects. Hydrometallurgy 109:116–124
7. Song CG, Zhang HL, Dong YM, Pei LL, Liu HH, Jiang JS, Xu HB (2021) Investigation on the fabrication of lightweight aggregate with acid-leaching tailings of vanadium-bearing stone coal minerals and red mud. Chin J Chem Eng 32:353–359
8. Bao SX, Qin L, Zhang YM, Luo YP, Huang XL (2021) A combined calcination method for activating mixed shale residue and red mud for preparation of geopolymer. Constr Build Mater 297:Article 123789
9. Gao LY, Yang XY, Wu YL, Chen YL, Tong LR (2023) Kinetics of alkali-dissolving desilication reaction of serpentine acid leaching slag[J]. Chin J Nonferrous Met 33:2718–2728 (in Chinese with English abstract)
10. Wu HF, Li JQ, Chen CY, Xia FL, Xie ZS (2020) Suspension calcination and alkali leaching of low-grade high-sulfur bauxite: Desulfurization, mineralogical evolution and desilication. Int J Min Met Mater 27:602–610
11. Mu WN, Lu XY, Cui FH, Luo SH, Zhai YC (2018) Transformation and leaching kinetics of silicon from low-grade nickel laterite ore by pre-roasting and alkaline leaching process. Trans Nonferrous Metal Soc 28:169–176
12. Wang RC, Zhai YC, Ning ZQ, Ma PH (2014) Kinetics of SiO_2 leaching from Al_2O_3 extracted slag of fly ash with sodium hydroxide solution. Trans Nonferrous Metal Soc 24:1928–1936
13. Gustavo DR, Alexander CJR, Rodolfo GW, Mario HR, Esquivel MR (2022) Optimization of combined mechanical activation-leaching parameters of low-grade α-spodumene/NaF mixture using response surface methodology. Miner Eng 184:Article 107633
14. Li L, Zheng Y, Yu Q, Jiao BQ, Li DW (2022) Optimization for enhanced electrokinetic treatment of air pollution control residues using response surface methodology focusing on heavy metals leaching risk and extractability. Process Saf Environ 159:534–546
15 Xin CF, Xia HY, Jiang GY, Zhang Q, Zhang LB, Xu YJ, Cai WC (2022) Mechanism and kinetics study on ultrasonic combined with oxygen enhanced leaching of zinc and germanium from germanium-containing slag dust. Sep Purif Technol 302:Article 122167
16 Wu Y, Pan XL, Han YJ, Yu HY (2019) Dissolution kinetics and removal mechanism of kaolinite in diasporic bauxite in alkali solution at atmospheric pressure. Trans Nonferrous Metal Soc 29:2627–2637
17. Deng RR, Xie ZM, Liu ZH, Tao CY (2019) Leaching kinetics of vanadium catalyzed by electric field coupling with sodium persulfate. Electroanal Chem 854:Article 113542
18. Md S, Rao KA, Sulekha M (2022) Influence of rheology in the filtration of leach slurry generated by alkaline pressure leaching of a limestone ore. Clean Chem Eng 4:Article100079

19. Kuenzel C, Ranjbar N (2019) Dissolution mechanism of fly ash to quantify the reactive aluminosilicates in geopolymerisation. Resour Conserv Recycl 150:Article 104421
20. Ji HY, Mi X, Tian QK, Liu CL, Yao JX, Ma SH, Zeng GS (2021) Recycling of mullite from high-alumina coal fly ash by a mechanochemical activation method: Effect of particle size and mechanism research. Sci Total Environ 784:Article 147100
21. Ikechukwu AN, Mabel K, Okechukwu DO (2023) Leaching for alumina recovery in hydrochloric acid solution. Sci Afr 23:e02045
22. Xiang L, Li XR, Cao PG, Luo J, Jing H (2024) Stepwise extraction and utilization of silica and alumina from coal fly ash by mild hydrothermal process. Process Saf Environ 182:918–929
23. Mehmet KT, Zümra BT, Nizamettin D (2022) Optimization of process parameters and kinetic modelling for leaching of copper from oxidized copper ore in nitric acid solutions. Trans Nonferrous Metal Soc. 32:1301–1313
24. Li HQ, Hui JB, Wang CY, Bao WJ, Sun Z (2014) Extraction of alumina from coal fly ash by mixed-alkaline hydrothermal method. Hydrometallurgy 147–148:183–187
25. Yang SL, Li Y, Jia DY, Yao K, Liu W (2017) The synergy of Box-Behnken designs on the optimization of polysaccharide extraction from mulberry leaves. Ind Crop Prod 99:70–78
26 Elemike EE, Onwudiwe DC, Abiola OK, Ibe KA (2018) Surface characterisation and reaction kinetics of silver nanoparticles mediated by the leaf and flower extracts of French marigold (Tagetes patula). IET Nanobiotechnol. 12:957–962
27 Xiong YT, Wang L, Wang L, Li S, Yang GH, Cao C, Liu SX, Nie YM, Jia LB (2023) Optimization and kinetic analysis of direct acid leaching of vanadium from converter vanadium slag under atmospheric pressure. Miner Eng 198:Article 108091
28. Chen ZY, Ye GH, Xiang PZ, Tao YY, Tang Y, Hu YJ (2022) Effect of activator on kinetics of direct acid leaching of vanadium from clay vanadium ore. Sep Purif Technol 281:Article 119937
29. Wu JH, Xiao Y, Yang XS, Xu DH, Zhang ZY, Zhong YJ, Wang XL (2022) Leaching kinetics for magnesium extraction from phosphate rock in the nitric acid method. Miner Eng 189:Article 107894
30. Kavcı E, Çalban T, Çolak S, Kuşlu S (2014) Leaching kinetics of ulexite in sodium hydrogen sulphate solutions. J Ind Eng Chem 20:2625–2631
31. Chen G, Jiang CL, Liu RL, Xie ZM, Liu ZH, Cen SD, Tao CY, Guo SG (2021) Leaching kinetics of manganese from pyrolusite using pyrite as a reductant under microwave heating. Sep Purif Technol 277:Article 119472
32. Ma ZY, Liu Y, Zhou JL, Liu MD, Liu ZZ (2019) Optimization of microwave assisted leaching of vanadium from spent catalyst based on response surface methodology. Chin J Nonferrous Metals 29:1308–1315 (in Chinese with English abstract)
33. Cifuentes B, Figueredo M, Cobo M (2017) Response surface methodology and Aspen Plus integration for the simulation of the catalytic steam reforming of ethanol. Catalysts 7:Article 15